Journal of Physics and Chemistry of Solids 132 (2019) 116–120

Contents lists available at ScienceDirect

Journal of Physics and Chemistry of Solids

journal homepage: www.elsevier.com/locate/jpcs

Femtosecond laser assisted synthesis of gold nanorod and graphene hybrids and its photothermal property in the near-infrared region

Yang Yu, Lihe Yan*, Jinhai Si, Yanmin Xu, Xun Hou

Key Laboratory for Physical Electronics and Devices of the Ministry of Education & Shaanxi Key Lab of Information Photonic Technique, School of Electronics & Information Engineering, Xi'an Jiaotong University, Xi'an, 710049, China

ARTICLE INFO

Keywords:
Composite materials
Nanostructured materials
Laser processing
Heat conduction

ABSTRACT

Gold nanorod (GNR) and reduced graphene oxide (rGO) hybrids are synthesized using photochemical method based on femtosecond laser ablation without the usage of strong chemical reducing agents. The products are characterized by absorption spectra, transmission electron microscopy (TEM) and X-ray photoelectron spectroscopy (XPS). The formed GNR are well located on the surface of rGO sheets. By adjusting the laser ablation time, the aspect ratio and optical properties of GNR can be well controlled. The produced nanocomposites exhibited an excellent near-infrared (NIR) photothermal performance with a photothermal conversion efficiency of 77.8%, suggesting that the hybrids have large potential as agents in photothermal therapy.

1. Introduction

Photothermal therapy (PTT) using laser radiation is an emerging field in cancer treatment. In PTT process, photothermal agents are employed to achieve the selective heating of the local environments. When the PTT agents absorb light, electrons are excited to the excited state from the ground state, and then relax through nonradiative decay. This results in the increase in the kinetic energy and overheating of the local environment around the light absorbing species, inducing the destruction of local cells or tissues. Compared with conventional surgical treatment of solid tumors, this technique has the advantages of short treatment time, few complications and short recovery time [1,2]. Finding suitable photothermal conversion materials is the core of PTT.

With the fast development of nanotechnology, varies of nanomaterials such as carbon based nanomaterials, two-dimensional nanomaterials and metal nanomaterials, have received widespread interest due to their unique optical properties [3–6]. For the use of photothermal conversion, a lot of nanomaterials with broad absorption band and excellent photothermal conversion efficiency have been synthesized, such as titanium oxide nanoparticles and tellurium nanoparticles [7,8]. However, lasers with wavelength located at 650–950 nm and 1000–1350 nm are usually used in the PTT to avoid the energy loss by the outer skin and tissues in human body [9,10]. For this reason, the suitable photothermal agents should have a high optical absorption efficiency and high photothermal conversion efficiency in the near-infrared (NIR) region. Among lots of nanomaterials, gold nanorod (GNR) draws much attention due to its tunable and strong absorption in NIR region [11–13]. To further extend the application of GNR, combinations with other materials are promoted. As a single-atom-thick sheet of hexagonally arrayed sp^2-bonded carbon atoms, graphene has attracted much attention due to its unique optical and thermal properties. Because of the large specific surface area, high thermal conductivity and electrical conductivity of graphene, GNR and graphene hybrids have been demonstrated to be a good platform for wider applications in a lot of areas, such as catalysis, electrochemical sensors, surface-enhanced Raman scattering and PTT [14–17].

The typical synthesis process of GNR based on chemical reactions usually contains two steps: the generation of gold nanoparticle seeds, and the growth and formation of the GNR from the seeds. In the second procedure, some drastic reactions are needed to reduce the Au ions, and strong chemical reducing agents such as $NaBH_4$ are usually used, which seriously affects the usage of the products especially in the biological areas. Although some green agents extracted from plants such as aqueous leaf extract of green tea and sucrose diluted are used to synthesize gold nanoparticles/rGO (AuNPs/rGO) nanostructure [18,19], the green synthesis of GNR/rGO nanostructure is still need to be improved. Photochemical synthetic strategies of nanomaterials have drawn much attention due to the great advantages of easy performing and environmental protection [20–25]. Femtosecond laser has been widely used in photochemical method to synthesize various nanomaterials such as metal nanoparticles and nanocomposites due to its unique properties of ultra-short pulse duration and ultra-high peak power

* Corresponding author.
E-mail address: liheyan@mail.xjtu.edu.cn (L. Yan).

https://doi.org/10.1016/j.jpcs.2019.04.020
Received 25 December 2018; Received in revised form 12 April 2019; Accepted 15 April 2019
Available online 16 April 2019
0022-3697/

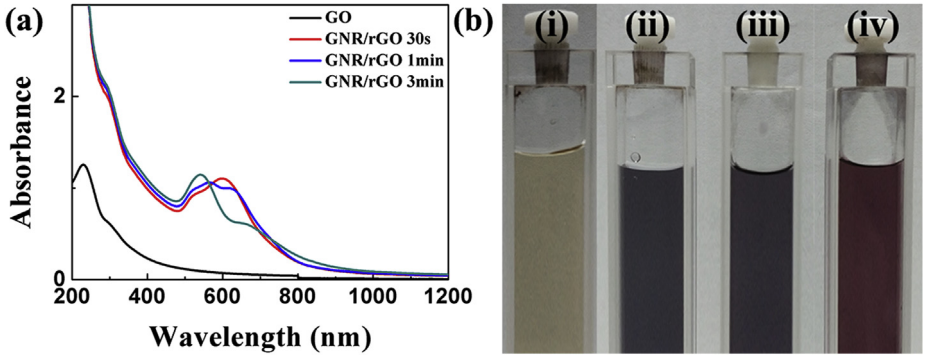

Fig. 1. The (a) absorption spectra and (b) pictures of (i) GO and GNR/rGO with ablation time of (ii) 30 s, (iii) 1 min and (iv) 3 min.

intensity [26,27]. When femtosecond laser pulses irradiate on graphene oxide (GO) aqueous solution mixed with metal ions, the reduction of the metal ions and GO might take place synchronously. This method could provide a new photochemical strategy to synthesize seeding gold nanoparticles for the formation of GNR and reduced graphene oxide (rGO) hybrids without the usage of harmful reducing agents such as $NaBH_4$.

Herein, we propose to synthesize GNR and rGO hybrids using the seeding gold nanoparticles prepared by femtosecond laser ablation method. The as-prepared GNR/rGO hybrids are characterized by absorption spectra, transmission electron microscopy (TEM) and X-ray photoelectron spectroscopy (XPS). By adjusting the ablation time during the laser reduction process, the aspect ratio of GNR can be well controlled. The photothermal properties of prepared GNR/rGO hybrids are investigated using a continuous-wave (CW) 808 nm diode laser. The results show that the GNR/rGO hybrids have an effective photothermal conversion efficiency of 31.5%, indicating a potential application in PTT.

2. Material and methods

2.1. Preparation of GNR/rGO

To synthesize to GNR/rGO hybrids, at first, 1 mg of GO with a size in the range of 0.5–5 μm was dispersed in 10 mL of distilled water with ultrasonic treatment for a few hours until a homogeneous yellow solution was obtained. Then, 1 mmol of hexadecyl trimethyl ammonium bromide (CTAB) was added, followed by stirring with water bath heating at 40 °C for about 15 min until the CTAB is completely dissolved. After that, 200 μL of 0.025 mmol mL^{-1} $HAuCl_4$ solution, 65 μL of 10 mmol mL^{-1} $AgNO_3$ solution and 70 μL of 100 mmol mL^{-1} ascorbic acid (AA) solution was added, followed by stirring with water bath heating at 30 °C for about 30 min.

A mode-locked Ti: sapphire laser with central wavelength of 800 nm, pulse width of 100 fs, and repetition rate of 1 kHz was used to prepare the Au nanoparticle seeds supported on graphene. 10 mL of solution was ablated by laser pulses. A shutter was used to control the number of the pulses injected into the solution. The laser was focused by a lens with a focal length of 100 mm and the pulse energy in use is 300 μJ. During the laser ablation process, a magnetic stirrer was used to make the solution to be ablated homogenously.

After laser ablation, the solution was put into a thermostat kept at 30 °C for about 3 h to complete the growth of the nanorods. Finally, the product was centrifuged at 10000 rpm for 10 min to remove the unreacted ions and redundant impurities. The obtained precipitate was redispersed in water for subsequent use.

2.2. Characterization

To study the characteristics of the hybrids, UV–Vis absorption spectra were performed using a UV-2600 spectrophotometer in a quartz cuvette. TEM and high resolution TEM (HRTEM) images were performed using a JEM-2100Plus microscope to study the morphology of the nanocomposites. XPS were performed using an ESCALAB Xi + XPS spectrometer.

2.3. Photothermal property

To study the photothermal conversion property of the products, a CW 808 nm diode laser was used. 2 mL of the solution was irradiated by the laser with a power of 0.5 W and an incident laser spot diameter of 8 mm for 10 min at a room temperature of 25 °C. A thermocouple was used to measure the temperature variation of the solution during the process.

3. Results and discussion

Following shows the results of our experiments. Firstly, GNR/rGO hybrids are synthesized using photochemical method with a femtosecond laser. The effect of the laser ablation time on the morphology of the products is systematically studied. Fig. 1(a) shows the absorption spectra of the as-prepared GO and GNR/rGO hybrids with ablation time varying from 30 s to 3 min. From the figure, two characteristic surface plasma resonance (SPR) peak of GNR can be obviously observed in the solutions, indicating the formation of GNR. The short-wavelength peak ranging from 520 nm to 540 nm is originated from the transversal surface plasma resonance (TSPR) of GNR and the long-wavelength peak at the range of 600 nm–700 nm is originated from the longitudinal surface plasma resonance (LSPR) of GNR, respectively [13,16]. From the absorption spectra, the TSPR peak has a little red-shift with increasing the ablation time of the laser pulses, which may be due to the attachment of GNR to the graphene sheets [16]. As reports in other works, when GNR was attached to rGO, the TSPR peak will have a red-shift [28]. With prolonging the laser irradiation time, the reduction degree of rGO is gradually increased, which might cause the red-shift of the TSPR peak. Because the LSPR peak is red-shifted with increasing the aspect ratio of GNR [29], the results indicated that the aspect ratio of GNR is increased with increasing the ablation time. Fig. 1(b) shows the picture of GO and GNR/rGO with different ablation time, a distinguished evolution of the color can be seen. The color of GO (inset (i) of Fig. 1(b)) is brown yellow, while the color of GNR/rGO changes from dark blue to dark purple and then dark red, with the ablation time increased from 30 s (inset (ii)), to 1 min (inset (iii)) and 3 min (inset (iv)).

The morphology variation of GNR/rGO hybrids with different ablation time is investigated by TEM, as shown in Fig. 2. Fig. 2(a), (b) and (c) show the TEM images of GNR/rGO with ablation time of 30, 1 min and 3 min, respectively. The GNR can be clearly seen in all images, indicating the formation of the GNR. Besides, graphene sheets with folds also can be seen from the images. As shown in Fig. 2(a), the

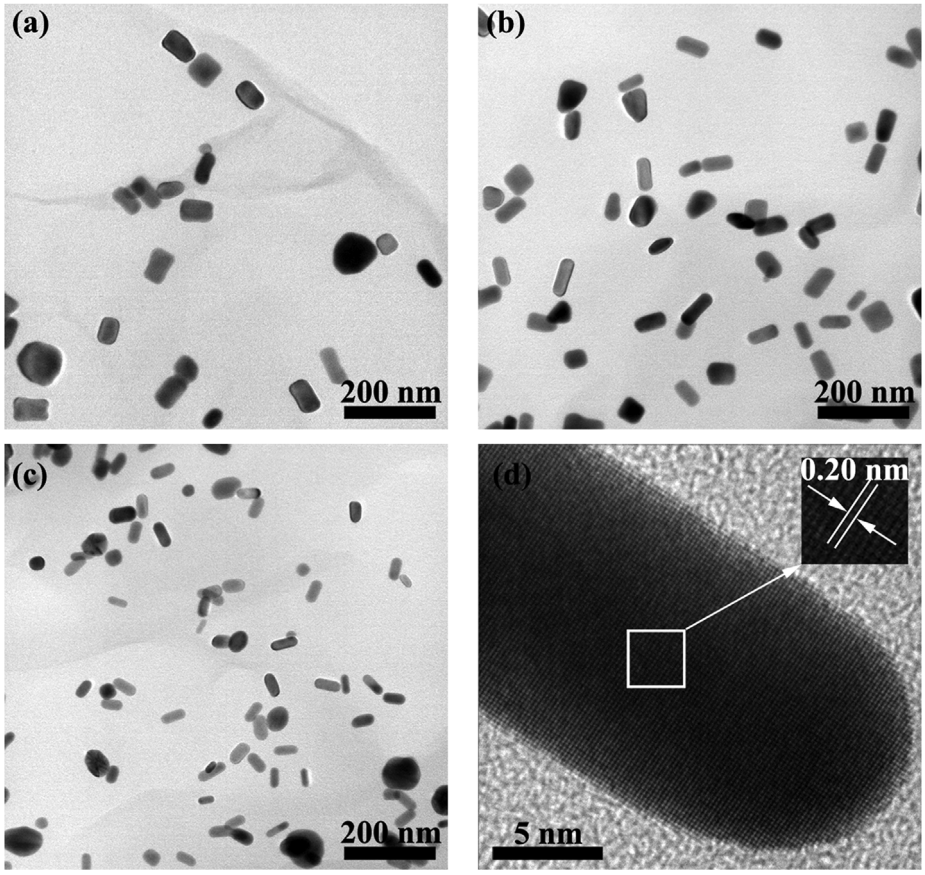

Fig. 2. The TEM images of GNR/rGO with ablation time of (a) 30 s (dashed line shows the edge of graphene), (b) 1 min and (c) 3 min; (d) the HRTEM image of GNR, inset shows the enlarged image of the square area.

dashed line is a visual guide of the edge of graphene sheets and the lower left area of the dashed line is the graphene sheets. The image shows that the GNR are well located on the surface of graphene sheets. Fig. S1 gives a lower-resolution TEM image showing the whole view of GNR/rGO hybrids, which has a relatively more clear edge of graphene sheets. Fig. 2(d) shows the high-resolution TEM (HRTEM) image of GNR. Obvious lattice fringes with the spacing of 0.20 nm which is attributed to the (200) plane of the Au crystallite can be observed [30].

Table 1 shows the average length, width and aspect ratio of GNR with different ablation time which is obtained from the TEM images in Fig. S2. By measuring the length and width of GNR in the images, we can obtain the corresponding distribution of length, width and aspect ratio of GNR/rGO with different ablation time. From the table, we can conclude that, with increasing the ablation time, the length and width is decreased, but the aspect ratio is increased. The increased aspect ratio is corresponding to the red-shifted LSPR peak in absorption spectra. During the growth process of GNR, the initial concentration of Au seeds is a main factor affecting the aspect ratio of GNR [29]. With increasing the ablation time, the initial concentration of Au seeds is increased, and the amount ratio of residual Au^{3+} ions used for the growth of GNR to the formed Au seeds is decreased. As a result, the length and width of the formed GNR is decreased when the ablation time of femtosecond laser is prolonged. On the other hand, the aspect ratio is increased at the beginning of growth process because the longitudinal growth rate of initial formed Au seeds is faster than the transversal growth rate [31]. When the aspect ratio is increased to a certain threshold, the GNR will grow along the transversal direction. At a short ablation time, the Au seeds is relatively few, so the excess Au^{3+} ions will grow along the transversal direction after the aspect ratio reach the threshold, as a result, the aspect ratio is decreased.

Table 1
The length, width and aspect ratio of GNR/rGO with different ablation time.

	Length (nm)	Width (nm)	Aspect Ratio
GNR/rGO 30 s	38.3	19.5	2
GNR/rGO 1 min	32.2	16.3	2.03
GNR/rGO 3 min	24.3	10.8	2.36

To further study the chemical structure of the products, GNR/rGO hybrids with different ablation time is investigated by XPS, as given in Fig. 3. Fig. 3(a) shows the C 1s XPS spectra of GO and GNR/rGO. Peaks centered at 284.5 and 286.6 eV are contributed to C=C and C-O groups, respectively [32,33]. The content of oxide is clearly reduced in GNR/rGO hybrids compared with GO, indicating the reduction of GO to rGO during the synthesis process. Fig. 3(b) shows the Au 4f XPS spectra of GNR/rGO. Peaks centered at 84 and 87.7 eV are corresponding to the binding energies of Au $4f_{7/2}$ and Au $4f_{5/2}$ of Au, respectively [34].

The temperature varies caused by the photothermal conversion of GO, rGO, GNR and GNR/rGO are studied using the CW 808 nm diode laser with a power of 0.5 W. 2 mL of the different solution is irradiated by the laser for 10 min, after then, the laser is shut off and the solution is cooling down to the room temperature. As shown in Fig. 4, the high photothermal conversion of GO, rGO, GNR and GNR/rGO for 808 nm light is clearly demonstrated by the comparison that of pure water under the same laser irradiation conditions.

Usually, the photothermal conversion efficiency, η_T, is used to characterize the phototermal property of materials, which is calculated using the equation [35,36].

$$\eta_T = \frac{hA(T_{max} - T_{surr}) - Q_0}{I(1 - 10^{-A_\lambda})} \quad (1)$$

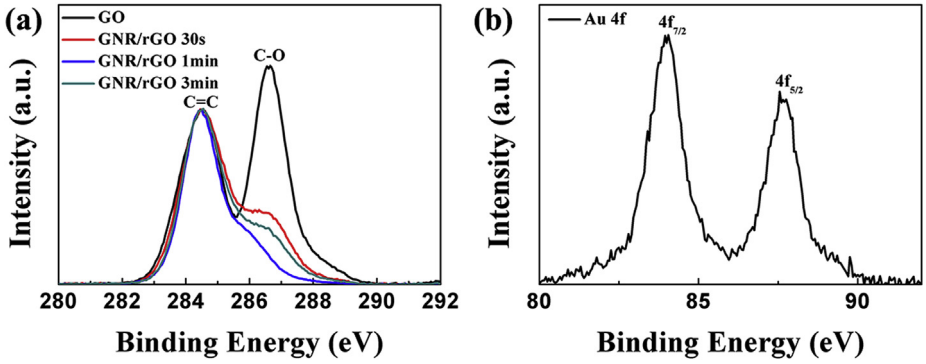

Fig. 3. The XPS spectra of (a) C 1s of GO and GNR/rGO with ablation time of 30 s, 1 min and 3 min; (b) Au 4f of GNR/rGO.

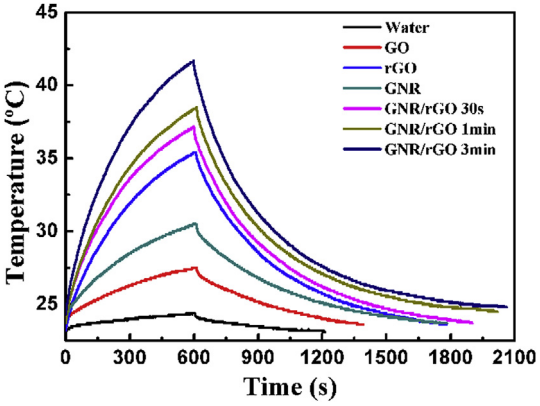

Fig. 4. The temperature varies of water, GO, rGO, GNR and GNR/rGO with ablation time of 30 s, 1 min and 3 min with laser irradiation of 10 min and after laser shut off.

where h is the heat transfer coefficient of the solution and A is the cross section area perpendicular to conduction. T_{max} and T_{surr} are the maximum temperature after 10 min laser irradiation and the surrounding temperature, respectively. Q_0 is the rate of heat dissipated by the solvent and cuvette due to light absorption. I is the irradiating laser power and A_λ is the absorbance of the sample at the excitation wavelength of 808 nm. The value of hA follows the equation

$$\tau_s = \frac{m_D C_D}{hA} \tag{2}$$

where τ_s is the sample system time constant. m_D and C_D are the mass and heat capacity of the solvent, respectively. In our experiment, m_D is 2 g and C_D is 4.18 J g^{-1} °C^{-1}. τ_s can be obtained using the time constant method from the cooling down curve after laser is shut off. Usually, the cooling process can be described using the equation

$$T - T_{surr} = (T_{max} - T_{surr}) exp\left(-\frac{t}{\tau_s}\right) \tag{3}$$

where t is the time after laser shut off and T is the temperature at the time of t. By doing logarithm, Equation (3) can be described as a linear function of t, and the value of τ_s can be calculated from the slope.

T_{max} and T_{surr} can be obtained from the temperature vary curves in Fig. 4. Q_0 can be obtained from the temperature vary curve of pure water in Fig. 4, which is calculated to be 44.2 mW. The value of $I(1-10^{-A_\lambda})$ means the power absorbed by sample which can be obtained by measuring the power before and after laser irradiated to the sample using power meter. Using Equations (1)–(3), we can calculated the photothermal conversion efficiency value of η_T. The value of maximum temperature change ΔT_{max}, sample system time constant τ_s and the photothermal conversion efficiency value of η_T of different samples are given in Table 2.

Table 2
The value of ΔT_{max}, τ_s and η_T of different samples.

	ΔT_{max} (°C)	τ_s (s)	η_T (%)
GO	3.9	347	23.8
rGO	12.2	376	56.4
GNR	6.8	399	38.8
GNR/rGO 30 s	13.5	362	60.4
GNR/rGO 1 min	14.8	389	61.2
GNR/rGO 3 min	17.4	352	77.8

The photothermal conversion efficiency of rGO and GNR is 56.4% and 38.8%, respectively, which is comparable to the results in some other reports [37–39]. When the rGO is decorated with GNR, we can see from the Fig. 4 that the maximum temperature is clearly increased, indicating the enhancement of photothermal conversion ability. The calculated photothermal conversion efficiency of GNR/rGO hybrids prepared by 30 s, 1 min and 3 min fs laser ablation are 60.4%, 61.2% and 77.8%, respectively. Compared with GO, rGO and GNR, the photothermal conversion efficiency of GNR/rGO hybrids is obviously increased. As the wavelength of 808 nm is near the LSPR peak of GNR in GNR/rGO hybrids, more light energy can be absorbed and converted into heat by the hybrids. Besides, because of the extremely high value of the thermal conductivity which is up to 5300 W mK^{-1} for graphene [40,41], the thermal energy can be effectively transferred to surrounding solutions. So, the GNR/rGO hybrids exhibit excellent photothermal conversion property.

4. Conclusions

In summary, the GNR/rGO hybrids are successfully synthesized by photochemical method using femtosecond laser pulses. The products are characterized by absorption spectra, transmission electron microscopy (TEM) images and X-ray photoelectron spectroscopy (XPS). The results show that the formed GNR are well located on the surface of rGO sheets and the aspect ratio of GNR can be well controlled by adjusting the laser ablation time. The photothermal property in the first NIR window is demonstrated using a CW 808 nm diode laser. The results show that the GNR/rGO hybrids display an excellent photothermal conversion property, indicating a potential application in PTT.

Conflicts of interest

There are no conflicts to declare.

Acknowledgements

This work was supported by National R&D Program of China (2017YFA0207400), and the National Natural Science Foundation of China (Grant No. 61690221, 11674260 and 11474078), Key Research

and Development Plan of Shaanxi Province with grant no. 2017ZDXM-GY-120, the Fundamental Research Funds for the Central Universities, and the collaborative Innovation Center of Suzhou Nano Science and Technology. The TEM work was performed at the International Center for Dielectric Research (ICDR), Xi'an Jiaotong University, Xi'an, China. The authors also thank Mr. Ma and Ms. Lu for their help in using TEM.

Appendix A. Supplementary data

Supplementary data to this article can be found online at https://doi.org/10.1016/j.jpcs.2019.04.020.

References

[1] S. Lal, S.E. Clare, N.J. Halas, Nanoshell-enabled photothermal cancer therapy: impending clinical impact, Accounts Chem. Res. 41 (2008) 1842–1851 https://doi.org/10.1021/ar800150g.
[2] J. Shao, H. Xie, H. Huang, Z. Li, Z. Sun, Y. Xu, Q. Xiao, X. Yu, Y. Zhao, H. Zhang, H. Wang, P.K. Chu, Biodegradable black phosphorus-based nanospheres for in vivo photothermal cancer therapy, Nat. Commun. 7 (2016) 12967 https://doi.org/10.1038/ncomms12967.
[3] C.N.R. Rao, A.K. Sood, K.S. Subrahmanyam, A. Govindaraj, Graphene: the new two-dimensional nanomaterial, Angew. Chem. Int. Ed. 48 (2009) 7752–7777 https://doi.org/10.1002/anie.200901678.
[4] G. Aragay, J. Pons, A. Merkoçi, Recent trends in macro-, micro-, and nanomaterial-based tools and strategies for heavy-metal detection, Chem. Rev. 111 (2011) 3433–3458 https://doi.org/10.1021/cr100383r.
[5] M.E. Vance, T. Kuiken, E.P. Vejerano, S.P. McGinnis, J.M.F. Hochella, D. Rejeski, M.S. Hull, Nanotechnology in the real world: redeveloping the nanomaterial consumer products inventory, Beilstein J. Nanotechnol. 6 (2015) 1769–1780 https://doi.org/10.3762/bjnano.6.181.
[6] K. Nakamura, T. Oshikiri, K. Ueno, Y. Wang, Y. Kamata, Y. Kotake, H. Misawa, Properties of plasmon-induced photoelectric conversion on a TiO_2/NiO p–n junction with Au nanoparticles, J. Phys. Chem. Lett. 7 (2016) 1004–1009 https://doi.org/10.1021/acs.jpclett.6b00291.
[7] C. Ma, J. Yan, Y. Huang, C. Wang, G. Yang, The optical duality of tellurium nanoparticles for broadband solar energy harvesting and efficient photothermal conversion, Sci. Adv. 4 (2018) eaas9894https://doi.org/10.1126/sciadv.aas9894.
[8] J. Yan, P. Liu, C. Ma, Z. Lin, G. Yang, Plasmonic near-touching titanium oxide nanoparticles to realize solar energy harvesting and effective local heating, Nanoscale 8 (2016) 8826–8838 https://doi.org/10.1039/C6NR01295G.
[9] A.M. Gobin, M.H. Lee, N.J. Halas, W.D. James, R.A. Drezek, J.L. West, Near-infrared resonant nanoshells for combined optical imaging and photothermal cancer therapy, Nano Lett. 7 (2007) 1929–1934 https://doi.org/10.1021/nl070610y.
[10] A.M. Smith, M.C. Mancini, S. Nie, Bioimaging: second window for in vivo imaging, Nat. Nanotechnol. 4 (2009) 710 https://doi.org/10.1038/nnano.2009.326.
[11] X. Huang, I.H. El-Sayed, W. Qian, M.A. El-Sayed, Cancer cell imaging and photothermal therapy in the near-infrared region by using gold nanorods, J. Am. Chem. Soc. 128 (2006) 2115–2120 https://doi.org/10.1021/ja057254a.
[12] M.R.K. Ali, Y. Wu, T. Han, X. Zang, H. Xiao, Y. Tang, R. Wu, F.M. Fernández, M.A. El-Sayed, Simultaneous time-dependent surface-enhanced Raman spectroscopy, metabolomics, and proteomics reveal cancer cell death mechanisms associated with gold nanorod photothermal therapy, J. Am. Chem. Soc. 138 (2016) 15434–15442 https://doi.org/10.1021/jacs.6b08787.
[13] M. Tsai, S.G. Chang, F. Cheng, V. Shanmugam, Y. Cheng, C. Su, C. Yeh, Au nanorod design as light-absorber in the first and second biological near-infrared windows for in vivo photothermal therapy, ACS Nano 7 (2013) 5330–5342 https://doi.org/10.1021/nn401187c.
[14] J. Song, X. Yang, O. Jacobson, L. Lin, P. Huang, G. Niu, Q. Ma, X. Chen, Sequential drug release and enhanced photothermal and photoacoustic effect of hybrid reduced graphene oxide-loaded ultrasmall gold nanorod vesicles for cancer therapy, ACS Nano 9 (2015) 9199–9209 https://doi.org/10.1021/acsnano.5b03804.
[15] Y. Kim, H. Na, Y.W. Lee, H. Jang, S.W. Han, D. Min, The direct growth of gold rods on graphene thin films, Chem. Commun. 46 (2010) 3185 https://doi.org/10.1039/c002002h.
[16] W. Bai, H. Huang, Y. Li, H. Zhang, B. Liang, R. Guo, L. Du, Z. Zhang, Direct preparation of well-dispersed graphene/gold nanorod composites and their application in electrochemical sensors for determination of ractopamine, Electrochim. Acta 117 (2014) 322–328 https://doi.org/10.1016/j.electacta.2013.11.175.
[17] C. Hu, J. Rong, J. Cui, Y. Yang, L. Yang, Y. Wang, Y. Liu, Fabrication of a graphene oxide–gold nanorod hybrid material by electrostatic self-assembly for surface-enhanced Raman scattering, Carbon 51 (2013) 255–264 https://doi.org/10.1016/j.carbon.2012.08.051.
[18] M. Šimšíková, M. Bartoš, P. Keša, T. Šikola, Green approach for preparation of reduced graphene oxide decorated with gold nanoparticles and its optical and catalytic properties, Mater. Chem. Phys. 177 (2016) 339–345 https://doi.org/10.1016/j.matchemphys.2016.04.036.
[19] R. Britto Hurtado, M. Cortez-Valadez, J.R. Aragon-Guajardo, J.J. Cruz-Rivera, F. Martínez-Suárez, M. Flores-Acosta, One-step synthesis of reduced graphene oxide/gold nanoparticles under ambient conditions, Arab. J. Chem. (2018), https://doi.org/10.1016/j.arabjc.2017.12.021.
[20] A.M. Morales, C.M. Lieber, A laser ablation method for the synthesis of crystalline semiconductor nanowires, Science 279 (1998) 208–211 https://doi.org/10.1126/science.279.5348.208.
[21] M. Dell'Aglio, R. Gaudiuso, O. De Pascale, A. De Giacomo, Mechanisms and processes of pulsed laser ablation in liquids during nanoparticle production, Appl. Surf. Sci. 348 (2015) 4–9 https://doi.org/10.1016/j.apsusc.2015.01.082.
[22] F. Kim, J.H. Song, P. Yang, Photochemical synthesis of gold nanorods, J. Am. Chem. Soc. 124 (2002) 14316–14317 https://doi.org/10.1021/ja028110o.
[23] D. Zhang, B. Gökce, S. Barcikowski, Laser synthesis and processing of colloids: fundamentals and applications, Chem. Rev. 117 (2017) 3990–4103 https://doi.org/10.1021/acs.chemrev.6b00468.
[24] J. Xiao, P. Liu, C.X. Wang, G.W. Yang, External field-assisted laser ablation in liquid: an efficient strategy for nanocrystal synthesis and nanostructure assembly, Prog. Mater. Sci. 87 (2017) 140–220 https://doi.org/10.1016/j.pmatsci.2017.02.004.
[25] D. Tan, X. Liu, Y. Dai, G. Ma, M. Meunier, J. Qiu, A universal photochemical approach to ultra-small, well-dispersed nanoparticle/reduced graphene oxide hybrids with enhanced nonlinear optical properties, Adv. Opt. Mater. 3 (2015) 836–841 https://doi.org/10.1002/adom.201400560.
[26] V. Nguyen, J. Si, L. Yan, X. Hou, Direct demonstration of photoluminescence originated from surface functional groups in carbon nanodots, Carbon 108 (2016) 268–273 https://doi.org/10.1016/j.carbon.2016.07.019.
[27] V. Nguyen, L. Yan, H. Xu, M. Yue, One-step synthesis of multi-emission carbon nanodots for ratiometric temperature sensing, Appl. Surf. Sci. 427 (2018) 1118–1123 https://dx.doi.org/10.1016/j.apsusc.2017.08.133.
[28] J. Huang, L. Zhang, B. Chen, N. Ji, F. Chen, Y. Zhang, Z. Zhang, Nanocomposites of size-controlled gold nanoparticles and graphene oxide: formation and applications in SERS and catalysis, Nanoscale 2 (2010) 2733 https://doi.org/10.1039/C0NR00473A.
[29] B. Nikoobakht, M.A. El-Sayed, Preparation and growth mechanism of gold nanorods (NRs) using seed-mediated growth method, Chem. Mater. 15 (2003) 1957–1962 https://doi.org/10.1021/cm020732l.
[30] X. Lu, L. Tao, D. Song, Y. Li, F. Gao, Bimetallic Pd@ Au nanorods based ultrasensitive acetylcholinesterase biosensor for determination of organophosphate pesticides, Sensor. Actuator. B Chem. 255 (2018) 2575–2581 https://doi.org/10.1016/j.snb.2017.09.063.
[31] C.J. Murphy, L.B. Thompson, D.J. Chernak, J.A. Yang, S.T. Sivapalan, S.P. Boulos, J. Huang, A.M. Alkilany, P.N. Sisco, Gold nanorod crystal growth: from seed-mediated synthesis to nanoscale sculpting, Curr. Opin. Colloid Interface 16 (2011) 128–134 https://doi.org/10.1016/j.cocis.2011.01.001.
[32] S. Moussa, G. Atkinson, M. SamyEl-Shall, A. Shehata, K.M. AbouZeid, M.B. Mohamed, Laser assisted photocatalytic reduction of metal ions by graphene oxide, J. Mater. Chem. 21 (2011) 9608 https://doi.org/10.1039/c1jm11228g.
[33] V. Abdelsayed, S. Moussa, H.M. Hassan, H.S. Aluri, M.M. Collinson, M.S. El-Shall, Photothermal deoxygenation of graphite oxide with laser excitation in solution and graphene-aided increase in water temperature, J. Phys. Chem. Lett. 1 (2010) 2804–2809 https://doi.org/10.1021/jz1011143.
[34] A.Y. Klyushin, T.C.R. Rocha, M. Hävecker, A. Knop-Gericke, R. Schlögl, A near ambient pressure XPS study of Au oxidation, Phys. Chem. Chem. Phys. 16 (2014) 7881 https://doi.org/10.1039/c4cp00308j.
[35] B. Li, Q. Wang, R. Zou, X. Liu, K. Xu, W. Li, J. Hu, $Cu_{7.2}S_4$ nanocrystals: a novel photothermal agent with a 56.7% photothermal conversion efficiency for photothermal therapy of cancer cells, Nanoscale 6 (2014) 3274 https://doi.org/10.1039/C3NR06242B.
[36] D.K. Roper, W. Ahn, M. Hoepfner, Microscale heat transfer transduced by surface plasmon resonant gold nanoparticles, J. Phys. Chem. C 111 (2007) 3636–3641 https://doi.org/10.1021/jp064341w.
[37] Z.M. Markovic, L.M. Harhaji-Trajkovic, B.M. Todorovic-Markovic, D.P. Kepić, K.M. Arsikin, S.P. Jovanović, A.C. Pantovic, M.D. Dramićanin, V.S. Trajkovic, In vitro comparison of the photothermal anticancer activity of graphene nanoparticles and carbon nanotubes, Biomaterials 32 (2011) 1121–1129 https://doi.org/10.1016/j.biomaterials.2010.10.030.
[38] O.A. Savchuk, J.J. Carvajal, J. Massons, M. Aguiló, F. Díaz, Determination of photothermal conversion efficiency of graphene and graphene oxide through an integrating sphere method, Carbon 103 (2016) 134–141 https://doi.org/10.1016/j.carbon.2016.02.075.
[39] Y. Ito, Y. Tanabe, J. Han, T. Fujita, K. Tanigaki, M. Chen, Multifunctional porous graphene for high-efficiency steam generation by heat localization, Adv. Mater. 27 (2015) 4302–4307 https://doi.org/10.1002/adma.201501832.
[40] A.A. Balandin, S. Ghosh, W. Bao, I. Calizo, D. Teweldebrhan, F. Miao, C.N. Lau, Superior thermal conductivity of single-layer graphene, Nano Lett. 8 (2008) 902–907 https://doi.org/10.1021/nl0731872.
[41] W. Yu, H. Xie, W. Chen, Experimental investigation on thermal conductivity of nanofluids containing graphene oxide nanosheets, J. Appl. Phys. 107 (2010) 94317 https://doi.org/10.1063/1.3372733.